Electron density distribution in ferromagnetic nickel: A γ-ray diffraction study

W. Jauch
Helmholtz-Zentrum Berlin für Materialien und Energie, Glienicker Strasse 100, D-14109 Berlin, Germany

M. Reehuis
Max-Planck-Institut für Festkörperforschung, Heisenbergstr. 1, D-70569 Stuttgart, Germany

(Received 25 August 2008; revised manuscript received 2 October 2008; published 11 December 2008)

High-accuracy single-crystal structure factors, complete up to $\sin\theta/\lambda = 1.9$ Å^{-1}, have been measured from ferromagnetic nickel at 295 K using 316.5-keV gamma radiation. The experimental uncertainty of the structure factors is of the order of 10 millielectrons per atom for all data. A detailed description of the electron density distribution is presented in terms of a multipolar atomic deformation model. Achievement of a reliable Debye-Waller factor is of vital importance in this context. The charge asphericity is due to an excess e_g orbital occupancy of 43.4(2)%. The 3*d* shell in the metal is contracted by 2.07(5)% relative to the free atom. The results are discussed and compared with earlier experimental and theoretical works. In contrast to bcc Cr and Fe, solid-state effects are less pronounced in fcc Ni. Clear disentanglement between the 3*d* and 4*s* valence electrons could be accomplished for the first time. The general expectation that the number of 3*d* electrons in the metal should be increased as compared to the atom was confirmed in the case of iron by combining spin and charge-density data. In the case of nickel, it is rejected as revealed by the γ-ray data alone. Only with the d^8 configuration, consistency is achieved between observed and refined mosaic widths of the sample crystal. A $3d^8$ configuration implies that the majority-spin *d* band cannot be full. Strong support is lent to a localized atomic character of the valence electrons.

DOI: 10.1103/PhysRevB.78.235113 PACS number(s): 61.05.cp, 71.20.Be, 61.66.Bi

I. INTRODUCTION

Experimental determination of the electron density distribution in a crystal, $\rho(\mathbf{r})$, relies on accurate values of x-ray structure factors, sampled from many diffracting planes. These basic quantities, the Fourier components of $\rho(\mathbf{r})$, are converted from the Bragg intensities and reflect the charge redistribution in the crystal-bound atoms. Since the changes in electron density upon bonding are generally quite small and may easily be masked by experimental deficiencies, data of genuine high quality are a crucial prerequisite. Although nickel has been a subject of charge-density-related experiments for a few decades now, the studies have been restricted to powders or to very few low-order data, and in fact no single-crystal examination has been reported. The aim of this work is to present an accurate electron density analysis of crystalline nickel. The experimental basis is an extended set of structure factors extracted from γ-ray Bragg diffraction intensities.

Heavier-atom structures, such as Ni, pose a special challenge and are much more demanding than those of organic systems since the heavier the element the smaller the fraction of scattering from the valence electrons relative to the core contribution. The accessible Q range (momentum transfer) is limited to the occurrence of Bragg reflections. For the elemental solids with their small and highly symmetrical unit cells, there are only few reflections in the low-Q region where valence scattering is concentrated, which must therefore be measured with exceptional accuracy. This lack of suitability accounts for the very limited number of x-ray diffraction results for the 3*d* transition metals.

The use of 316.5-keV gamma radiation offers two basic advantages in removing major sources of systematic error. The first advantage is the high photon energy, being the reason for low absorption and extinction, no dispersion corrections, and allowance of large samples making surface effects negligible. The second advantage is due to favorable experimental conditions besides energy, such as the perfect stability, homogeneity, and monochromaticity ($\Delta\lambda/\lambda = 10^{-6}$) of the incident γ-ray beam. Because of the relatively low intensity, the γ-ray technique is confined to small-unit-cell systems. It is noteworthy that the photon energy used in this work is considerably beyond 100 keV presently employed in synchrotron-radiation charge-density studies.

The methodical advantages of γ-ray diffraction in experimental electron density analysis have been realized during the past years in exhaustive studies of archetypal compounds such as the antiferromagnetic transition-metal monoxides and difluorides.[1] The present work is a sequel to our investigations of chromium[2] and α-iron.[3]

II. EXPERIMENTAL AND DATA REDUCTION

Nickel has a face-centered-cubic structure (space group $Fm\bar{3}m$; $a = 3.523\,87$ Å at 298 K).[4] The single crystal used in the present investigation was a cube of dimensions $2.58 \times 2.59 \times 2.60$ mm^3, purchased from MaTecK/Jülich (Germany).

Double-crystal γ-ray diffraction, using a perfect Si crystal as a collimator with an angular resolution of 1.5 s of arc, was employed to measure diffraction profiles along three perpendicular directions. An angular full width at half maximum (FWHM) varying between 2.55 and 2.64 min of arc was found. In a diffraction experiment, the width of the rocking curve contains contributions from lattice strain ($\Delta d/d$) as well as lattice tilt (mosaicity η). The relation is $(\Delta\theta)^2 = (\Delta d/d)^2 \tan^2\theta + \eta^2$, where θ is the Bragg angle. Due to the

short wavelength of γ radiation, the Bragg angles are very small and the first term is negligible. The measured rocking curves are therefore a direct mapping of the mosaic distribution function of the crystal under investigation. The correction for secondary extinction is governed by the mosaic width of the sample, which is treated in the data analysis as an adjustable parameter. In the following, comparison between fitted and observed mosaicities will play a crucial role in the assessment of results.

The diffraction data have been collected on the four-circle gamma-ray diffractometer installed at the Hahn-Meitner-Institut, where the most intense line of a ^{192}Ir source ($T_{1/2}$ =73.83 d) with a wavelength of 0.0392 Å (316.5 keV) is used. The flux at the sample position from a 200 Ci source amounts to 10^6 photons/s/cm^2. The angular profiles of the diffraction peaks were recorded in ω-step scan mode (120 steps of length 0.01°) with an intrinsic germanium detector. The data set, complete up to sin θ/λ=1.9 Å^{-1}, was collected at room temperature. The data collection lasted 14 weeks.

Simultaneous reflection is an unwanted effect (Renninger effect), which occurs if for some crystal orientation two or more reciprocal-lattice points lie on the Ewald sphere simultaneously. In general, it will cause a diminution of the observed intensity of strong reflections. It can be detected by measurements at different azimuthal settings ψ around the diffraction vector. Although for short wavelengths multiple diffraction seems to be unavoidable, its occurrence is largely eliminated by the narrow wavelength spread of the incoming γ-ray beam. However, simultaneous reflection effects may be enhanced by crystal-specific properties such as high symmetry or large structure factor magnitudes. Variations in intensities among symmetry-equivalent reflections appreciably exceeding the counting statistical scatter can be ascribed to simultaneous reflection. Perturbations of equivalent reflections were indeed observed. The nine strongest reflections including symmetry-related equivalents were therefore measured at different ψ angles. Significant intensity diminution was found for the very strongest reflections 111, 200, and 220, each of them sampled by 40 measurements (ψ-settings × equivalents). The corresponding data, identified as contaminated by multiple reflection, were discarded.

A total of 446 diffraction data were eventually used, corresponding to 86 independent reflections with an unprecedented counting-statistical precision of $\Sigma\sigma(I)/\Sigma I$=0.0024 for the averaged data. The structure factor uncertainty is ≤13 millielectron per atom, approaching the precision of Pendellösung fringe measurements on perfect crystals. The absorption correction (μ=1.001 cm^{-1}) [5] resulted in a transmission range from 0.774 to 0.792. The absorption-weighted mean path lengths through the sample varied between 2.304 and 2.557 mm. It was therefore considered necessary to process each reflection with its individual path length in the calculation of the extinction correction and to treat symmetrically equivalent reflections separately. Data reduction was carried out using the XTAL suite of crystallographic programs.[6]

The data were corrected for the contribution of inelastic thermal diffuse scattering (TDS) from the acoustic phonons to the total intensity using the formalism of Skelton and Katz.[7] Due to the short wavelength of gamma radiation, (i) the Bragg angles are very small and (ii) the ω-scan mode is used. (iii) The detector aperture was circular. Under these three special conditions, the TDS correction factor, defined by $I_{\mathrm{TDS}}=\alpha I_{\mathrm{Bragg}}$, reduces to the simple form, α =const $k_{\mathrm{B}}T\rho^{-1}\langle v^{-2}\rangle[1-\cos(\Delta\omega/2)]^{1/2}(\sin\theta/\lambda)^3$, where const=$32\pi\sqrt{2}$, ρ is the density, $\langle v^{-2}\rangle$ is the mean reciprocal square velocity of sound, and $\Delta\omega$ is the total angular range of the Bragg peak. It is independent of the size of the detector window, and for a uniform intensity profile ($\Delta\omega$=0.70°), the only variable quantity is the momentum transfer. The sound velocities were taken from Ref. 8. The maximum correction factor was α=0.16.

III. RESULTS

Structure refinements were performed with the program system VALRAY,[9] minimizing $\chi^2=\Sigma w(|F_o|^2-|F_c|^2)^2$, where F_o and F_c are the observed and calculated structure factors, respectively. The observations are weighted by their counting-statistical variances. The classical form factor approximation of nonrelativistic scattering theory is used. A brief exposure of the relevance of relativistic effects is given in Ref. 2 and will not be repeated here.

Except for Cr and Cu, the free 3d atoms have $3d^n4s^2$ electronic ground-state configurations. In going to the metal, the number of 4s electrons is commonly assumed to be close to $3d^{n+1}4s$ based on band theoretical results.[10] In the case of iron, the metallic configuration has indeed been supported by γ-ray diffraction results.[3] For the charge-density analysis of Ni, both configurations $3d^84s^2$ ($^3F_4$) and $3d^94s$ ($^3D_3$) will be applied, with the scattering factors calculated from the Hartree-Fock (HF) wave functions given in Clementi and Roetti.[11]

A. Independent-atom model

The adjustable parameters are the scale factor k of the observed structure factors ($k^{-1}|F_o|=|F_c|$), the secondary extinction parameter g using the Becker-Coppens formalism,[12] and the harmonic mean-square vibrational amplitude U. The observed structure factor contains a contribution from the nuclear Thomson scattering amplitude, $f_N=(Ze)^2/Mc^2$. For nickel, f_N=0.00733 electron units, which is not negligible at a millielectron precision level and has to be taken into account.

A reliable scale factor is crucial for a physically meaningful determination of the charge density. Least-squares refinements based only on high-order reflections strongly reduce the influence of deformations in the outer shell, and the cutoff value for the minimum sin θ/λ should be as large as possible. On the other hand, U is positively correlated with k such that the high-order data set should be as large as possible. A threshold of sin $\theta/\lambda\geq$0.7 Å^{-1} yields the correlation coefficient corr(k,U)=0.88, whereas corr(k,U)=0.94 for sin $\theta/\lambda\geq$1.0 Å^{-1} even though the data extend to 1.9 Å^{-1}. Choosing sin $\theta/\lambda\geq$0.7 Å^{-1}, the least-squares fit yielded k =1.0030(6). From the observed mosaic spread, it is predicted that there are still noticeable contributions from extinction ($y=I_{\mathrm{obs}}/I_{\mathrm{kin}}\geq$0.994) which have been accounted for.

TABLE I. Quality of fit for the various $3d^8$ scattering models based on 446 observations; Np=number of adjustable parameters. In all cases, the scale factor was fixed to the value obtained from a high-order refinement ($\sin\theta/\lambda > 0.7$ Å^{-1}).

	IAM	Monopole	Multipole
χ^2	3957	1932	1340
Np	2	3	4

TABLE II. Mean-square vibrational amplitude and multipole model parameters of nickel at room temperature. Reliability factors for the 446 observations: $R(F)=\Sigma\|F_o-F_c\|/\Sigma\|F_o\|=0.0031$ and $wR(F^2)=[\Sigma w(F_o^2-F_c^2)^2/\Sigma wF_o^4]^{1/2}=0.0048$.

U (Å^2)	0.004 72(1)
κ	1.0207(5)
$P_4(\|e\|$Å$^4)$	0.131(7)

The validity of the independent-atom model (IAM) estimate of k was assessed by the more elaborate multipole model (to be discussed below), now using all data. Since the VALRAY program allows inclusion of k as a fit parameter only for the IAM, it had to be estimated otherwise. Trial values of k were chosen, and χ^2 was minimized at each point with respect to all other parameters except for g which was fixed at its measured value. The increase in the overall minimum, $\Delta\chi^2=1$, corresponds to a one-standard-deviation departure from the least-squares estimator. The result is $k=1.0027(3)$. There is thus agreement between both scaling procedures, giving confidence in the estimate of the very narrow statistical error, $\sigma(k)/k=0.03\%$.

B. Multipole model

In the aspherical atom multipole model the electron density is decomposed into a small series of nucleus-centered real spherical harmonic functions.[13] The model charge density of Ni is divided into four components of the core and the 4s electrons, as well as the spherical and aspherical parts of the 3d valence shell;

$$\rho_{\mathrm{Ni}}(\mathbf{r}) = \rho_{\mathrm{core}}(r) + \rho_{4s}(r) + \kappa^3\rho_{3d}(\kappa r) + \mathrm{P}_4\kappa^3\rho_4(\kappa r)\mathrm{K}_4(\mathbf{r}/r).$$

For site symmetry $m\bar{3}m$ the lowest nonvanishing higher pole is the Kubic harmonic $\mathrm{K}_4(\mathbf{r}/r)$ which is a linear combination of y_{40} and y_{44+}.

ρ_{core}, ρ_{4s}, and ρ_{3d} are HF densities of the appropriate atomic orbitals. The radial function of the hexadecapole, ρ_4, is constructed from a 3d3d atomic orbital product. The population coefficient P_4 and the radial expansion-contraction factor κ are variable parameters. A single κ parameter is used for both the monopole and the hexadecapole. This constraint is necessary for the subsequent calculation of 3d-orbital occupancies (see Sec. IV B). The global Cartesian frame is oriented parallel to the unit-cell axes.

In Table I, the quality of fit is given for the reference scattering models. The IAM results in a very high value of χ^2. A large improvement of fit is obtained with a spherical atom model allowing for a contraction of the 3d shell. Addition of the higher multipolar deformation leads to a further improvement of ~30% in χ^2. The data thus strongly support the multipole model, also reflected by the narrow confidence limits of the fit parameters which are listed in Table II. Figure 1 shows the static model deformation density (aspherical components only). The charge asphericity will be further discussed in Sec. IV C.

Adjustment of the secondary extinction parameter gives a Gaussian mosaic width (FWHM) of 2.601(6) min of arc, in perfect agreement with the observed value, convincingly demonstrating that extinction has been treated properly. The maximum reduction in $|F_o|^2$ is 15.7%, and a total of three independent reflections have a reduction up to 5%. Extinction is further discussed in Sec. IV D 3.

Transition-metal atoms require a multipole expansion at least up to $l=4$. Due to the high point symmetry, only the hexadecapole term K_{41} is allowed. Employment of only one function may be regarded as an intrinsic limitation of the

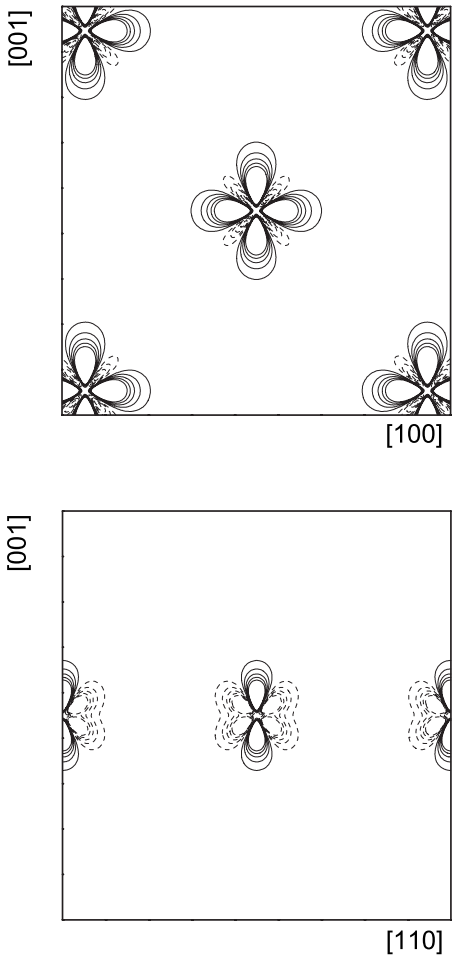

FIG. 1. Aspherical contributions to the static model density. Top: (100) plane (4×4 Å^2) with a density range from −0.45 to 1.78 e Å^{-3}. Bottom: (110) plane (5×5 Å^2) with a density range from −1.19 to 1.78 e Å^{-3}. Solid lines represent regions of excessive density and dashed lines represent depleted regions in steps of 0.1 e Å^{-3}. The zero contour is omitted. The densities are truncated at ±0.5 e Å^{-3}.

multipolar expansion. The next higher symmetry-allowed Kubic harmonic function is K_{61}, which is a linear combination of y_{60} and y_{64+}. Its inclusion with a single Slater function, $r^6 \exp(-\alpha r)$ with the standard exponent $\alpha = 8.35$ bohr^{-1}, led to a vanishing population parameter P_6, both for fixed and refined exponential parameters.

IV. DISCUSSION

A. Vibrational parameter

The mean-square amplitude of atomic vibrations obtained in this work is $U=0.004\,72(1)$ Å^2. Neglect of the TDS correction would have resulted in an artificial reduction in U by 6%.

It is interesting to compare the obtained value with the results of other methods that have been used in the determination of the nickel vibrational parameter at ambient temperature. Measurement of x-ray high-order powder reflections at two temperatures led to $U=0.004\,60(15)$ and $0.004\,89(15)$Å^2.[14,15] Refinement of single-crystal neutron-diffraction data gave $U=0.004\,67(5)$Å^2.[16] The values, $0.004\,83(10)$ and $0.004\,71$ Å^2, were derived from force constant models fitted to inelastic neutron-scattering data.[17,18] There is thus remarkable agreement between the independent estimates of U.

The possible influence of anharmonic contributions to the Debye-Waller factor has been investigated. For $m\bar{3}m$ point symmetry there is one isotropic and one anisotropic quartic term in the Gram-Charlier expansion of the atomic probability density function. Combined multipole-anharmonicity refinement leads only to an insignificant improvement of fit. There is thus no noticeable anharmonic component in the atomic potential which was also indicated by neutron-diffraction results.[16]

An adequate description of thermal motion is a necessary condition for a meaningful extraction of charge-density information from the diffraction data. Validation of the thermal parameter is therefore an important issue lending credence to the further conclusions.

B. Asphericity of charge distribution

The $3d$ electron density of a transition-metal atom may be described by spherical harmonic functions or, alternatively, it may be expressed in terms of the orbital components of its atomic wave function. By equating the two descriptions of the density, a set of linear equations is obtained from which the orbital occupancies can be derived from the multipole populations ($l_{\max}=4$).[19] In a cubic environment, the d wave functions decompose into doubly degenerate, e_g, and triply degenerate, t_{2g}, orbitals. The t_{2g} orbitals point along the body diagonal direction while the e_g orbitals are directed along the cube edges.

From the refined multipole parameters follows a fraction of 56.6(2)% t_{2g} and 43.4(2)% e_g, corresponding to the electron counts $n(t_{2g})=4.52$ and $n(e_g)=3.48$. The population of the t_{2g} orbitals is thus smaller than 3/5, the value for spherically symmetric d orbitals. The orbital occupancies are clearly reflected in the deformation map (Fig. 1) where the dominant features are electron buildup along ⟨100⟩. The symmetry character of the charge asphericity in fcc Ni is different from that observed in the bcc systems Cr and Fe with their preference of t_{2g} symmetry. The number of d electrons which contribute to the aspherical charge density is given by $Z_a=|n(t_{2g})-\frac{3}{2}n(e_g)|$; the deduced value is $Z_a=0.69(3)$.

In the fcc metals there occur pairs of reflections with different wave vectors of equal magnitude such as (511/333) or (600/442), and differences of the intensity ratios from unity are a direct measure of the anisotropy in the charge density. From measurement of three reflection pairs, the aspherical charge in Ni was estimated to be $Z_a=0.70(28)$.[20] There is thus agreement concerning a preponderance of e_g over t_{2g} charge density, with the present work providing a substantial advance in accuracy.

C. Form factors

1. X-ray radial 3d form factor

For the radial scaling parameter, κ, a highly significant deviation from the IAM is observed (40σ). The $3d^8$ valence shell exhibits a spatial contraction of 2.1% which corresponds to a form-factor expansion relative to the free atom. A solid-state orbital contraction is in line with our earlier studies of Cr and Fe. The contraction, however, is much less than in the bcc metals. Since the (111) reflection in Ni occurs at the same $\sin\theta/\lambda$ value as the (110) reflection in Cr and Fe, one may directly compare, for the first reflection of each metal, the ratio of the crystal scattering factor to the appropriate free-atom value, $f/f_{\mathrm{IAM}}=1.021$, 1.018, and 1.003 for Cr, Fe, and Ni, respectively.

For an fcc crystal, the atomic form factor f_{hkl} is related to the fitted structure factor F_{hkl} through $F_{hkl}=4(f_{hkl}+f_N)\mathrm{e}^{-M}$, where f_N accounts for nuclear Thomson scattering, and the effect of thermal motion reduces to the multiplicative Debye-Waller factor. Absolute values of the atomic crystal scattering factor for the first 15 diffraction vectors are listed in Table III, where also the numerical contributions of both the core and valence electrons have been individually identified. For fcc nickel, very few good crystal form factors are available from the literature which can be compared with the present results.

Inkinen *et al.*[21] used a powder sample and Mo $K\alpha$ radiation to measure all reflections within $\sin\theta/\lambda<1.3$ Å^{-1} on absolute scale resulting in scattering factors (corrected for TDS and dispersion) that are systematically reduced by about 1% with respect to our results. The possible error in the determination of the absolute scale was estimated to be about 1.5%. There is thus agreement within this error margin.

High-energy electron diffraction allows determination of the structure factor for a first-order reflection by exploiting the critical-voltage effect. Owing to the destructive interference, the intensity of the second-order reflection will show a minimum for a particular accelerating voltage. The first-order value is determined from the measured voltage by many-beam calculations covering higher-order Fourier coefficients for which the independent-atom approximation has

TABLE III. Static scattering factors from the multipole model fit for nickel in units of e/atom. f_{core} and $f_{valence}$ denote the contributions from the core (including 4s) and $3d^8$ valence electrons, respectively. f is the total contribution from all electrons. f_{IAM} is calculated from Ref. 11 for a $3d^8 4s^2$ independent atom, and f_{theory} is taken from Ref. 24.

hkl	$\sin\theta/\lambda$(Å^{-1})	f_{core}	$f_{valence}$	f	f/f_{IAM}	f/f_{theory}
111	0.2458	15.589	5.030	20.619	1.003	1.009
200	0.2838	14.934	4.415	19.349	1.005	1.014
220	0.4013	12.921	2.701	15.622	1.005	1.014
311	0.4706	11.794	1.961	13.755	1.006	1.013
222	0.4915	11.472	1.730	13.202	1.003	1.010
400	0.5676	10.398	1.223	11.621	1.010	1.013
331	0.6185	9.770	0.852	10.622	1.003	1.010
420	0.6345	9.587	0.802	10.389	1.006	1.011
422	0.6951	8.964	0.516	9.480	1.003	1.009
511	0.7373	8.587	0.429	9.016	1.009	1.010
333	0.7373	8.587	0.349	8.936	1.000	1.006
440	0.8026	8.084	0.206	8.290	1.002	1.006
531	0.8394	7.839	0.145	7.984	1.003	1.007
600	0.8513	7.765	0.190	7.955	1.011	1.011
442	0.8513	7.765	0.099	7.864	0.999	1.006

to be assumed. Two x-ray scattering factors have been determined, $f(111)=20.48(12)$ (Ref. 22) and $f(200)=19.17(17)$ (Ref. 23), which agree with the present values within standard deviation.

A comprehensive band-structure calculation for ferromagnetic nickel was performed by Wang *et al.*,[24] who used the computed wave functions to determine the x-ray form factor, tabulated up to $\sin\theta/\lambda=0.85$ Å^{-1}. In Table III, it is shown that the theoretical values are consistently lower by about 1% than the model fit values. Another *ab initio* calculation, based on the Green's-function method,[25] gave form factors up to 1% smaller than those calculated in Ref. 26.

By way of summary, the present crystal form factor of fcc Ni does not deviate considerably from earlier experimental or theoretical results. The situation is thus quite different from the case of the bcc metals Cr and Fe where substantial discrepancies have been observed.

2. Modeling of 4s electrons

The 4s electrons have a diffuse distribution of mean radius $\langle r\rangle=1.62$ Å, and at $\sin\theta/\lambda=0.25$ Å^{-1}, where the lowest-order Bragg reflection can be measured, the scattering factor has fallen to a small negative value of $f(4s)=-0.033$ electrons. Nevertheless, refinements with and without the inclusion of 4s electrons result in a rather striking difference. A deterioration of χ^2 by 12.0% occurs for $3d^8 4s^0$ relative to $3d^8 4s^2$. If the 4s electrons are completely delocalized implying a uniform charge density, they will not contribute to the Bragg intensities since the form factor is a delta function at $Q=0$. The configuration with two free electrons can thus be clearly distinguished from a localized model, the latter being supported on the basis of the χ^2 values.

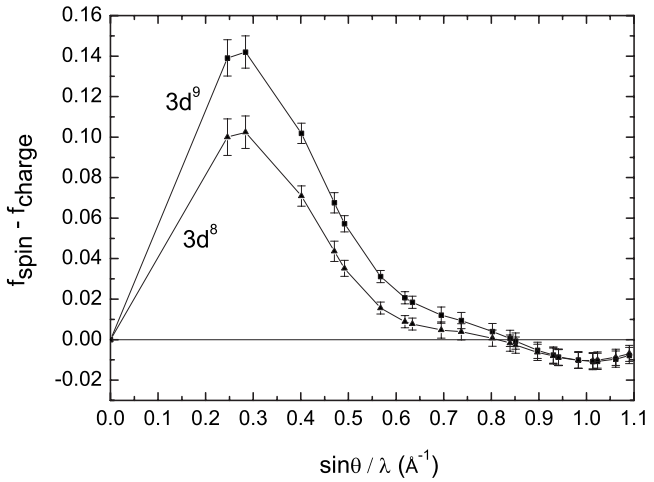

FIG. 2. The difference between the spherically averaged spin form factor ($=\langle j_o\rangle_{obs}$ from Ref. 27) and the radial charge form factors for $3d^9$ ($\kappa=1.021$) and $3d^8$ ($\kappa=1.020$) as deduced from neutron and γ-ray diffraction. The form factors are normalized to unity at $\sin\theta/\lambda=0$.

Application of an adjustable radial scaling parameter κ' for the outer s-electron shell yields $\kappa'=0.985(13)$. Simultaneous refinement of κ' and a population parameter of the form $3d^{8+n}4s^{2-n}$ yields the very small value $n=0.007(8)$ and $\kappa'=0.986(12)$. Although the influence of the 4s scattering is limited to the very low-order data, well-defined values are obtained, owing to exceptional accuracy. No deviation from the IAM is thus found by separate 4s electron fitting despite the large overlap. The mean $4s^2$ density in the interatomic region is constant and about 0.2 e Å^{-3}.

D. Number of 3d electrons

1. Quality of fits

Assuming the electron configuration $3d^9 4s^1$ ($^3D_3$) with Hartree-Fock wave functions from Clementi and Roetti[12] resulted in an increase in χ^2 by $\Delta\chi^2=19.0\%$ relative to the atomic ground-state configuration $3d^8 4s^2$ ($^5F_4$). The different d-electron counts are associated with the mean IAM radii $\langle r(d^8)\rangle=0.511$ Å and $\langle r(d^9)\rangle=0.554$ Å. There is thus statistical indication in favor of d^8 which, however, is insufficient for a strong conclusion based on physical ground. Additional information has to be incorporated.

2. Magnetic form factor

Complementary information about the spatial distribution of the unpaired 3d electrons is available from magnetic form-factor measurements. The magnetic form factor of ferromagnetic nickel has been thoroughly investigated by means of elastic scattering of polarized neutrons.[16,26] The asphericity of the spin density is found to be inverse to that of the charge density, with the unpaired d electrons showing a t_{2g} occupation of 77.6(4)%,[16] which is close to Mook's original value of 81(1)%.[26] A quantitative comparison between charge and spin form factor must therefore rely on the spherically averaged components. In Fig. 2, the comparison

is shown for a single $3d$ electron from the two different atomic configurations under consideration. As can be seen, there are substantial systematic differences between f_{spin} and f_{charge}.

In the ordinary Hartree-Fock method, electrons in the same shell but differing in spin are required to have the same radial wave function. This constraint is relaxed in the unrestricted HF (UHF) method for open-shell systems, which allows different radial functions for electrons with opposite spin, i.e., $R_{nl\alpha} \neq R_{nl\beta}$. For an atom with unbalanced spin, the UHF atomic functions are contracted for majority (α) spins relative to minority (β) spins: $\langle r(\alpha)\rangle < \langle r(\beta)\rangle$.

The Silverman-Obata sum rule[28] connects the spherical form factor with the average value of r^{-1}: $\int_0^\infty f(q)dq = \frac{\pi}{2}\langle r^{-1}\rangle$. Inspection of Fig. 2 shows that the predicted inequality $\langle r^{-1}\rangle_{\text{spin}} > \langle r^{-1}\rangle_{\text{charge}}$ is satisfied for both occupation numbers, d^8 and d^9, and does not allow a choice of the physical solution.

In our recently reported analysis of the charge distribution in α-Fe, joint interpretation of the charge and spin form factor has revealed that only the occupation Fe($3d^7$) is consistent with the spin-polarization effect predicted by the UHF method. For the configuration Fe($3d^6$), a compensation of positive and negative form-factor differences is observed, which would imply the same mean extension of the spin and charge distributions.

3. Exploiting extinction

Besides the microscopic electronic and thermal motion parameters, the least-squares model includes an extinction parameter, g, which concurrently is experimentally accessible. For an isotropic Gaussian mosaic distribution of FWHM Δ, $g = 0.6643/\Delta$ in units of rad^{-1}. As pointed out above, perfect agreement is obtained between the refined parameter, g[=878(2) rad^{-1}], and its observed value when the configuration d^8 is assumed. For the configuration d^9, the deterioration in χ^2 is associated with $g = 1077(2)$ rad^{-1} differing from observation by 100σ. It is therefore not surprising that fixing g at the observed value turns the least-squares fit way off to the huge value of $\chi^2 = 15\,534$. The inescapable conclusion is that only d^8 is compatible with the extinction present in the sample crystal.

At first sight, it seems to be astounding that extinction, which is commonly considered as a nuisance, in this case should be a source of knowledge. Our reliance in the validity of the mosaic crystal theory, worked out by Zachariasen[29] and by Becker and Coppens,[12] is based on stringent tests, performed with four γ-ray wavelengths in the energy range between 200 and 600 keV, which have confirmed and substantiated a number of important predictions, such as path length and wavelength dependencies.[30,31] It should be emphasized that these tests were independent of theoretical structure-factor estimates. Close agreement between observed and refined mosaic spreads was always achieved in our previous γ-ray studies performed over the years.

One of the advantages of using high-energy γ rays comes from the absence of primary extinction so that the problematic disentanglement between primary and secondary types is avoided, as may be seen straightaway. The boundary between mosaic crystal and perfect crystal theory is set by the extinction length, $t_{\text{ext}} = V/(\lambda F)$, ($V$=unit-cell volume, λ =wavelength, and F=structure factor in units of scattering length) and its magnitude with respect to the size of the perfect microdomains. The primary-extinction correction may be approximated by $y_p \approx \exp[-(\delta/2)^2]$, where δ is the average domain size in units of t_{ext}.[32] The perfect domains are expected to be of the order of 1 μm in diameter. In the present γ-ray study, the smallest value of t_{ext} is 49 μm for the (111) reflection. For a perfect block of thickness one tenth of t_{ext}, the intensity is reduced by 0.25% relative to the kinematical value. Hence, if there were perfect regions of $\sim$5 μm diameter, then primary extinction could introduce an apparent form-factor error of $\sim$0.06%. This has to be contrasted with $t_{\text{ext}} = 2.7$ μm for Mo $K\alpha$ radiation (17.4 keV), where primary extinction will necessarily occur, irrespective of the use of single crystal or powder material. The widely held position to tacitly ignore primary extinction is certainly unwarranted.

TABLE IV. Distribution of majority-spin and minority-spin $3d$ electrons in ferromagnetic nickel. The following γ-ray and neutron-diffraction (Ref. 16) results have been used: $n_\alpha(e_g)+n_\beta(e_g)=3.475$, $n_\alpha(t_{2g})+n_\beta(t_{2g})=4.525$, $n_\alpha(e_g)-n_\beta(e_g)+n_\alpha(t_{2g})-n_\beta(t_{2g})=0.648$, $n_\alpha(e_g)-n_\beta(e_g)=0.145$, and $n_\alpha(t_{2g})-n_\beta(t_{2g})=0.503$. The theoretical results are taken from Ref. 35.

	$n(t_{2g})$		$n(e_g)$		Total d	
	Present	Theory	Present	Theory	Present	Theory
Majority	2.51	2.77	1.81	1.87	4.32	4.63
Minority	2.01	2.29	1.67	1.70	3.68	3.98
Difference	0.50	0.48	0.15	0.17	0.65	0.65

4. Consequences for d-band filling

The spin magnetic moment per atom for solid Ni is $\sim 0.6\mu_B$. The integer number of 8 d electrons is therefore incompatible with a completely filled majority-spin band. The assumption of a complete subband filling leads to the conclusion that there are rather 9.4 d electrons per atom. This view was once quite common and is still encountered in the modern literature.[33,34]

Combination of the results from γ ray and neutron diffraction allows us to deduce the distribution of the $3d$ electrons with majority and minority spin among the two symmetry states. It is presented in Table IV, together with theoretical results. It should be noted that the band calculation gives less than five majority-spin electrons even though the total number of d electrons is obtained as 8.62.[35]

5. Metallic bond characteristics

The topological approach to chemical bonding[36] is considered to be a useful interpretation tool, according to which the bonding interaction is characterized by the density and its Laplacian, $\rho(\mathbf{r}_c)$ and $\nabla^2\rho(\mathbf{r}_c)$, at the bond critical saddle points, $\mathbf{r}_c$, between two nuclei. Metals are expected to show low values of $\rho(\mathbf{r}_c)$ and a slowly varying electron density

TABLE V. Characteristics of the bond critical point midway between nearest neighbors. $\lambda_{\|}$ denotes the curvature of $\rho(\mathbf{r}_c)$ along the internuclear line. Values of ρ in e Å^{-3}, values of $\nabla^2\rho(\mathbf{r}_c)$ and $\lambda_{\|}$ in e Å^{-5}. G, V, and G/ρ are given in atomic units.

	$\rho(\mathbf{r}_c)$	$\nabla^2\rho(\mathbf{r}_c)$	$\lambda_{\|}$	$G(\mathbf{r}_c)$	$V(\mathbf{r}_c)$	$G(\mathbf{r}_c)/\rho(\mathbf{r}_c)$
Ni($3d^8 4s^2$)	0.279	1.88	2.65	0.0272	−0.0349	0.659
Ni($3d^9 4s^1$)	0.228	2.42	3.33	0.0269	−0.0287	0.796
Fe($3d^7 4s^1$)	0.227	2.57	3.66	0.0279	−0.0290	0.829
Cr($3d^5 4s^1$)	0.237	2.79	4.03	0.0301	−0.0312	0.858

throughout the valence region with the Laplacian being dominated by the positive curvature along the bond path, $\nabla^2\rho(\mathbf{r}_c)>0$. The Laplacian is directly connected to the kinetic energy density $G(\mathbf{r}_c)$ and the electronic potential energy density $V(\mathbf{r}_c)$ that can be calculated using the density-functional approximation for $G(\mathbf{r}_c)$ (Ref. 37) in combination with the local virial theorem.

In an fcc lattice, there is only one unique bond path with the bond critical point midway between nearest neighbors. Its characteristics are summarized in Table V for nickel in both the $3d^8 4s^2$ and $3d^9 4s^1$ configurations. For ease of comparison, corresponding values from our previous studies of the bcc metals, chromium and α-iron, have also been included. Besides a positive Laplacian, typical metallic features include a low kinetic energy per electron, $G(\mathbf{r}_c)/\rho(\mathbf{r}_c)<1$ (in atomic units). Remarkably, the bond critical-point data are quite similar, largely independent of lattice type or the number of $3d$ electrons. Distinguished differences are due to the $4s$ electrons. There is approximate balance of kinetic and potential energies for the $4s^1$ configurations, whereas for $4s^2$, $|V|$ is found to be larger than G. This difference in local properties, revealed by the topological approach, seems to be lacking of observational consequences as it cannot be related to a measurable physical parameter.

V. CONCLUDING REMARKS

The present γ-ray data set is of unprecedented resolution and precision and has provided the most accurate representation of the electron density distribution in ferromagnetic nickel possible to date. Important findings include the following: (i) validation of data quality and scale factor estimate by comparison with available values of the thermal vibrational parameter; (ii) the $3d$ shell exhibits a contraction relative to the free atom, which is less pronounced than in the bcc metals Cr and Fe; (iii) the charge asphericity is small with a preference for e_g symmetry; (iv) clear disentanglement between the $3d$ and $4s$ valence electrons could be achieved; (v) the metallic configuration is d^8 rather than d^9; (vi) the majority-spin d band is not completely filled; and (vii) a localized atomic character of the $3d$ electrons is strongly supported. Finally, a study such as the present one recommends itself for calibration of theoretical methods.

ACKNOWLEDGMENTS

We thank H.-J. Bleif for helpful discussions. Support from the Deutsche Forschungsgemeinschaft (Grant No. UL164/4) is acknowledged.

[1] W. Jauch and M. Reehuis, Phys. Rev. B **65**, 125111 (2002); **67**, 184420 (2003); **70**, 195121 (2004); W. Jauch, Acta Crystallogr., Sect. A: Found. Crystallogr. **60**, 397 (2004).
[2] W. Jauch and M. Reehuis, Phys. Rev. B **73**, 085102 (2006).
[3] W. Jauch and M. Reehuis, Phys. Rev. B **76**, 235121 (2007).
[4] R. W. G. Wyckoff, *Crystal Structures*, 2nd ed. (Interscience, New York, 1963), Vol. 1.
[5] J. H. Hubbell and S. M. Seltzer, National Institute of Standards and Technology Internal Report No. 5632, 1995 (unpublished); also available via http://www.physics.nist.gov/PhysRefData/XrayMassCoef/cover.html
[6] *Computer Code XTAL 3.4, User's Manual*, edited by S. R. Hall, G. S. D. King, and J. M. Stewart (University of Western Australia, Perth, 1995).
[7] E. F. Skelton and J. L. Katz, Acta Crystallogr., Sect. A: Cryst. Phys., Diffr., Theor. Gen. Crystallogr. **25**, 319 (1969).
[8] G. W. C. Kaye and T. H. Laby, *Tables of Physical and Chemical Constants*, 15th ed. (Longman, London, UK, 1993).
[9] R. F. Stewart, M. Spackman, and C. Flensburg, *Computer Code VALRAY, User's Manual* (Carnegie-Mellon University, Pittsburgh/University of Copenhagen, Copenhagen, 2000).
[10] R. E. Watson, M. L. Perlman, and J. F. Herbst, Phys. Rev. B **13**, 2358 (1976).
[11] E. Clementi and C. Roetti, At. Data Nucl. Data Tables **14**, 177 (1974).
[12] P. J. Becker and P. Coppens, Acta Crystallogr., Sect. A: Cryst. Phys., Diffr., Theor. Gen. Crystallogr. **31**, 417 (1975).
[13] R. F. Stewart, Acta Crystallogr., Sect. A: Cryst. Phys., Diffr., Theor. Gen. Crystallogr. **32**, 565 (1976).
[14] M. V. Linkoaho, Philos. Mag. **23**, 191 (1971).
[15] T. Paakkari, Acta Crystallogr., Sect. A: Cryst. Phys., Diffr., Theor. Gen. Crystallogr. **30**, 83 (1974).
[16] P. J. Brown, J. Deporte, and K. R. A. Ziebeck, J. Phys. I **1**, 1529 (1991).
[17] H. W. T. Barron and T. Smith, J. Phys. Chem. Solids **27**, 1951 (1966).
[18] J. L. Feldman, J. Phys. Chem. Solids **30**, 367 (1969).
[19] A. Holladay, P. Leung, and P. Coppens, Acta Crystallogr., Sect. A: Found. Crystallogr. **39**, 377 (1983).
[20] C. Rocchi and F. Sacchetti, Solid State Commun. **96**, 771 (1995).
[21] O. Inkinen and P. Suortti, Ann. Acad. Sci. Fenn., Ser. A6 **147** (1964).
[22] D. Watanabe, R. Uyeda, and A. Fukuhara, Acta Crystallogr., Sect. A: Cryst. Phys., Diffr., Theor. Gen. Crystallogr. **25**, 138 (1969).
[23] T. Arii, R. Uyeda, O. Terasaki, and D. Watanabe, Acta Crystallogr., Sect. A: Cryst. Phys., Diffr., Theor. Gen. Crystallogr. **29**,

295 (1973).
[24] C. S. Wang and J. Callaway, Phys. Rev. B **15**, 298 (1977).
[25] S. Wakoh and J. Yamashita, J. Phys. Soc. Jpn. **30**, 422 (1971).
[26] H. A. Mook, Phys. Rev. **148**, 495 (1966).
[27] S. Kaprzyk, B. van Laar, and F. Maniawski, J. Magn. Magn. Mater. **23**, 105 (1981).
[28] J. N. Silverman and Y. Obata, J. Chem. Phys. **38**, 1254 (1963).
[29] W. H. Zachariasen, Acta Crystallogr. **23**, 558 (1967).
[30] A. Palmer and W. Jauch, Acta Crystallogr., Sect. A: Found. Crystallogr. **51**, 662 (1995).
[31] W. Jauch and A. Palmer, Acta Crystallogr., Sect. A: Found. Crystallogr. **58**, 448 (2002).
[32] P. Suortti, Acta Crystallogr., Sect. A: Cryst. Phys., Diffr., Theor. Gen. Crystallogr. **38**, 642 (1982).
[33] N. Ishimatsu, H. Maruyama, N. Kawamura, M. Suzuki, Y. Ohishi, and O. Shimomura, J. Phys. Soc. Jpn. **76**, 064703 (2007).
[34] R. Skomski, *Simple Models of Magnetism* (Oxford University Press, Oxford, 2008).
[35] S. Wakoh and J. Yamashita, J. Phys. Soc. Jpn. **25**, 1272 (1968).
[36] R. F. W. Bader, *Atoms in Molecules: A Quantum Theory* (Clarendon, Oxford, 1990).
[37] Yu. A. Abramov, Acta Crystallogr., Sect. A: Found. Crystallogr. **53**, 264 (1997).